MOF-derived Ni-WxC/carbon catalysts: Application to cellulose conversion into glycols

Joseph Boulos, Firat Goc, Maya Marinova, Noémie Perret, Franck Rataboul, Sebastien Royer, Jeremy Dhainaut

RESEARCH ARTICLE

MOF-derived Ni-W_xC/carbon catalysts: Application to cellulose conversion into glycols

Joseph Boulos,[a] Firat Goc,[b] Maya Marinova,[c] Noémie Perret,[b] Franck Rataboul,[b] Sébastien Royer,*[a] and Jérémy Dhainaut*[a]

[a] J.Boulos, Dr. S. Royer, Dr. J. Dhainaut
Univ. Lille, CNRS, Centrale Lille, Univ. Artois, UMR 8181 - UCCS - Unité de Catalyse et Chimie du Solide, F-59000 Lille, France
E-mail: sebastien.royer@univ-lille.fr ; jeremy.dhainaut@univ-lille.fr

[b] Dr. F. Goc, Dr. N. Perret, Dr. F. Rataboul
Univ. Lyon, Université Claude Bernard Lyon, CNRS, IRCELYON, 2 Av. Albert Einstein, F-69626 Villeurbanne, France

[c] Dr. M. Marinova
Univ. Lille, CNRS, INRA, Centrale Lille, Univ. Artois, FR 2638 – IMEC – Institut Michel-Eugène Chevreul, 59000 Lille, France

Supporting information for this article is given via a link at the end of the document.

Abstract: In this work, a series of Ni-W_xC/carbon materials have been prepared from a MOF precursor, DUT-8(Ni), following different tungsten deposition routes. After pyrolysis, nickel-tungsten alloys and tungsten carbide phases over nitrogen-doped carbons were obtained. These materials were applied to cellulose hydrogenolysis, where molar yields of up to 46 % in ethylene glycol (EG) and 9 % in propylene glycol (PG) were obtained at 245 °C after 1 hour of reaction time. The best performing catalyst demonstrated promising stability, as the EG yield remained constant over 3 recycling tests and very little nanoparticles sintering was observed.

Introduction

The one-pot hydrogenolysis of cellulose into diols - low carbon polyols (C2,3), ethylene glycol (EG), and propylene glycol (PG) -, which are prevailing intermediates in the manufacture of plastics, pharmaceuticals, food additives, and cosmetics, remains challenging as it involves 3 subsequent reactions: cellulose hydrolysis into glucose, retro-aldol condensation, and hydrogenation. Thus, catalysts presenting Lewis acidity and hydrogenating sites are required.[1] Owing to its Pt-like behavior, supported tungsten hemicarbide on activated carbon (60 % W_2C/AC) gave EG yields up to 29 % starting from cellulose.[2] The addition of nickel (2 % Ni-30 % W_2C/AC), an hydrogenating metal catalyst, further increased the EG yield up to 60 %.[2] In this line, we have recently shown that a 5 % Ni-30 % W_2C/AC catalyst gave EG and PG yields of 60 % and 10 %, respectively.[3] After three cycles, the EG yield decreased to 50 % while the PG yield remained constant. Moreover, the replacement of cellulose by raw pine wood led to similar yields.[3]

By replacing AC with a mesoporous carbon, smaller particles consisting of a mixture of tungsten carbide and hemicarbide (42 % WC_x/MC) were obtained and the EG yield was further increased to 72.9 %.[4] However, the EG yield rapidly decreased to 57.3 % after three cycles due to surface oxidation of W_xC into WO_x.[4]

Another way to control the size of the final W_xC particles is by using a cage-confinement pyrolysis strategy.[5] Starting from metal-organic frameworks (MOFs) with high surface areas and a metal center (Zr, Zn) that can be sublimated at high temperature, tungsten carbide nanoparticles (NPs) deposited on porous carbon were obtained.[5-6] Moreover, the carbon inherits the shape of the MOF (prismatic fibers, polyhedral or rhombododecahedral) and some of its porosity, as the dimensions shrink. Moreover, Yang et al. prepared Ni-W_xC/C nanofiber catalysts, in situ fabricated through the pyrolysis of (Ni, W)-impregnated ZnBTC MOF. Applied to the direct hydrogenolysis of cellulose, the EG and PG yields reached 34.1 % and 5.3 %, respectively.[7] Of note, the carbonization of organic linkers constituting the MOF allows to stabilize the framework metal clusters or ions into small NPs.[8] Herein, our objective was to directly prepare Ni-W_xC/C materials from the pyrolysis of a Ni-based MOF onto which the W phase was deposited by impregnation following two different routes, illustrated in Figure 1.

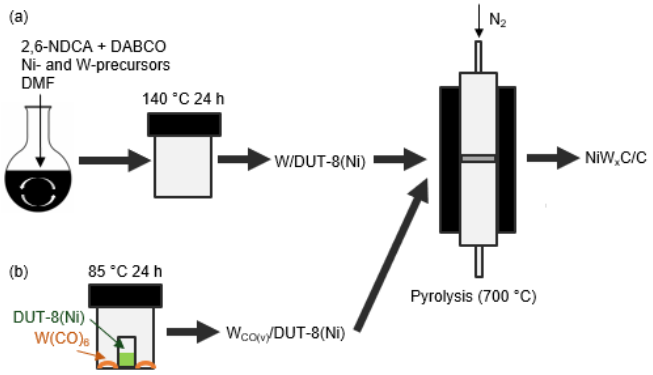

Figure 1. Graphic representation of the two routes evaluated to prepare NiW_xC/carbon catalysts: (a) liquid-mediated incorporation, and (b) chemical vapor deposition.

Results and Discussion

Preparation and pyrolysis of W/DUT-8(Ni)

DUT-**8**(Ni) has been selected as a good candidate as it presents a large surface area (above 1900 $m^2.g^{-1}$) and the following chemical composition: $Ni_2(C_{12}H_6O_4)_2(C_6H_{12}N_2)$.[9] After pyrolysis of DUT-8(Ni), a nitrogen-doped carbon containing about 23 % nickel is expected to be obtained. While the Ni content is much higher than previous studies (2-5 %), it remains one of the lowest than can be reached starting from a stable MOF structure. For the sake of simplicity, characterization and extensive discussion about the DUT-8(Ni) MOF as well as W/DUT-8(Ni) materials (theoretical W/Ni molar ratio = 0.3) are provided in SI (Figures S1-S7 and Tables S1-S2). Of note, XRD patterns (Fig. S2) reveal that only the chemical vapor deposition route ($W_{CO(v)}$/DUT-8(Ni)) preserved the crystalline structure of DUT-8(Ni), while additional reflections appear following the liquid-mediated incorporation (W_{NaO}/DUT-8(Ni) and $W_{CO(l)}$/DUT-8(Ni)). In line with this observation, aggregates of W-species are observed in W_{NaO}/DUT-8(Ni) and $W_{CO(l)}$/DUT-8(Ni) by SEM (Figs. S5-S6). This is due to the direct addition of tungsten precursors in the preparation mixture of DUT-8(Ni) and thus their impact over its crystallization process. Nonetheless, all materials present high surface areas (Fig. S3 and Tab. S2), above 1438 $m^2.g^{-1}$ (against 2067 $m^2.g^{-1}$ for the as-made DUT-8(Ni)).

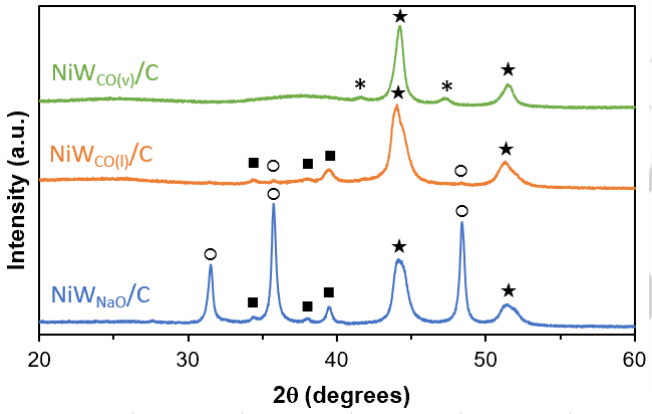

Figure 2. XRD diffractograms of pyrolyzed Ni-W_xC/C samples. ★: W_xNi_{1-x} (x = 0.04-0.06), ■: W_2C, ○: WC, *: C.

Table 1 presents the Ni and W contents of the Ni-W_xC/C catalysts after pyrolysis. Following the liquid-mediated incorporation route, lower W/Ni than expected were obtained and especially when using $W(CO)_6$ as the precursors remained in solution and were extracted following centrifugation. In any case, after pyrolysis high metal contents are obtained (71.2-78.4 % of the material) including 38.9-52.3 % of Ni. Figure 2 displays the XRD diffractograms of the pyrolyzed Ni-W_xC/carbon materials, showing a clear influence of the tungsten deposition route and precursor over the crystalline species formed. The presence of NiW alloys, and especially $Ni_{0.96}W_{0.04}$ but also $Ni_{0.94}W_{0.06}$ in the case of $NiW_{CO(l)}$/C, is observed in all materials. Their presence is a good hint about the proximity of some Ni and W species. No other crystalline phase is observed in the case of $NiW_{CO(v)}$/C, while WC and W_2C are observed in the materials prepared following the liquid-mediated incorporation route and especially in NiW_{NaO}/C. This underlines both the successful carburization of W species under N_2 and the ultrasmall size of these W species in the material prepared by the vapor deposition route. The average nanoparticle diameters were determined using the Scherrer equation and are presented in Table S3. The NiW alloys present small sizes between 8 and 12 nm, while the W_xC particles are sligthly bigger, from 13 nm ($NiW_{CO(l)}$/C) up to 24 nm (NiW_{NaO}/C).

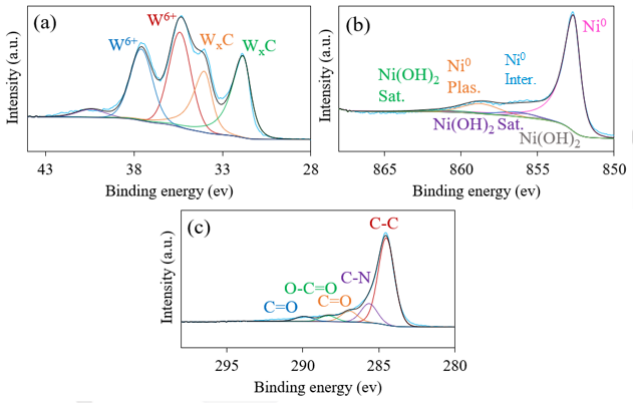

Figure 3. XPS surveys of $NiW_{CO(v)}$/C: (a) W 4f, (b) Ni 2p, and (c) C 1s.

XPS measurements were performed in order to identify the electronic environment of metals (W, Ni) as well as their oxidation states. The XPS spectra of the passivated samples, displayed in Figures 3 and S8, exhibit the core level signals for W 4f, Ni 2p, and C 1s. Of note, W_2C cannot be differentiated from WC by XPS. Moreover, WO_3 has non-stoichiometric properties, since its lattice withdraws a significant number of oxygen vacancies.[10] Hence, two main tungsten species are detected for all materials: W_xC ($4f_{7/2}$: 31.46 eV and $4f_{5/2}$: 33.64 eV), and W^{6+} ($4f_{7/2}$: 35.6 eV, $4f_{5/2}$: 37.78 eV). The presence of W^{6+} implies that for all materials, tungsten is mostly oxidized on the surface (≥ 70 % of W^{6+}, see Table S4) after passivation. Two oxidation states of Ni are also observed in the Ni 2p surveys: metallic nickel Ni^0 ($2p_{3/2}$: 852.6 eV with a surface plasmon loss peak at 858.7 eV and a weak intra-band transitions peak at 856.3 eV), and the oxidized nickel species, Ni^{2+} ($2p_{3/2}$: 854.9 eV and 5 satellites: 855.7 eV, 857.7 eV, 860.5 eV, 861.5 eV, and 866.5 eV).[11] The small shifts of binding energy observed between the different materials might stem from the formation of a Ni-N-C structure.[12] Unlike tungsten, metallic nickel remains the main phase after passivation (88-98 %, see Table S4). On the contrary, in a previous study we have shown that after passivation Ni^0 only represented 9% of the total nickel.[3] This suggests that the presence of residual carbon from the organic linker can protect the nickel phase toward reoxidation. Moreover, the asymmetrical C 1s peak of the XPS spectra at 284.5 eV (C-N) implies a considerable modification of the sp2 carbon atoms on the support surface (Figure 3). It is attributed to the carbonization of nitrogen, either from the organic linker or from the atmosphere, during pyrolysis at 700 °C. A signal around 283.5 eV, which is the C 1s carbide signature,[13] is also expected, but it is probably merged with the intense C-C bonds photopeak. The rest of the C 1s peaks are usually assigned to oxygen-containing

carbonaceous bands (C=O and O-C=O).[14] According to XPS, the surface of $NiW_{CO(v)}/C$ is thus composed of W_xC and Ni^0, which are not detected by XRD, as well as Ni^{2+} and W^{6+} which are likely to form NiW alloys after reduction as observed by XRD.

Table 1. Metal content and surface area of the NiW_xC/C materials.

Material	W (wt%)	Ni (wt%)	S_{BET} ($m^2\ g^{-1}$)
NiW_{NaO}/C	31.5	46.9	95
$NiW_{CO(l)}/C$	18.9	52.3	112
$NiW_{CO(v)}/C$	33.9	38.9	104

After pyrolysis, all materials exhibited a strong decrease of their surface area (95-112 $m^2.g^{-1}$, Table 1) along with an increase in pore diameters towards the mesopores region (2-24 nm, see Figure S9 and Table S5). As expected, the thermal treatment induced a collapse of the parent microporosity, occurring during the DUT-8 structure loss and reflected by a shift from type I to type II isotherms. The strong modifications of textural properties are also clearly associated to the high metallic content of the materials as prior seen.

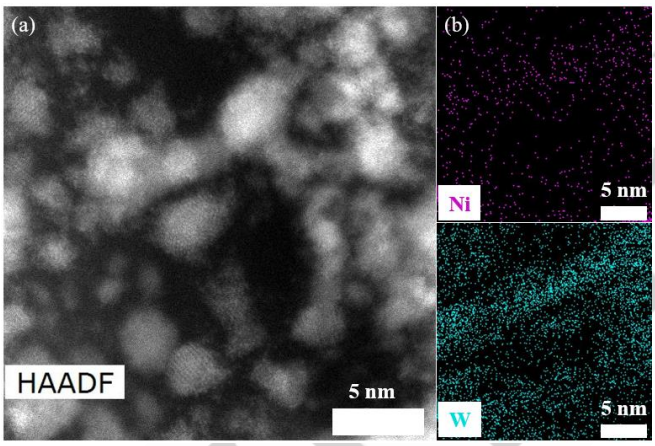

Figure 4. (a) HAADF-STEM and (b) related TEM-EDS elemental mapping images of $NiW_{CO(v)}/C$.

The morphology of the pyrolyzed materials were further examined by SEM and TEM. The morphology of DUT-8 crystals is partially preserved (Figures S10-S12), with angular particles of 200-800 nm forming larger aggregates of few microns. The brighter particles are W species, forming particles as big as 200 nm in the case of NiW_{NaO}/C (Figure S10). From XRD patterns, it may be attributed to WC. On the contrary, small W-containing NPs (estimated in the 5-35 nm interval, with an average size of 25 nm) homogeneously dispersed on the surface of aggregates can be observed for $NiW_{CO(v)}/C$ in Figure S12.

Among the different materials, $NiW_{CO(v)}/C$ presented the smallest particles size (average NP size of 2.7 nm) as observed by aberration-corrected scanning transmission electron microscopy (STEM), with a homogeneous dispersion of W and Ni particles throughout the analyzed samples (Figures 4 and S13), which is favorable for the possible synergy between the 2 metals. However, it should be mentioned that bigger Ni-based particles, around 50 nm, are also found (Figure S14). Lower dispersion of the Ni and W elements are obtained with the materials prepared by liquid-mediated incorporation. Indeed, NiW_{NaO}/C presents an average particle size of 13.8 nm, however with a satisfying proximity between Ni and W species, as identified by EDS elemental mapping (Figure S15). An even slightly larger average metal particles size is obtained for $NiW_{CO(l)}/C$ (~15 nm, see Figure S16). But on the contrary to NiW_{NaO}/C, significant segregation between Ni and W species is observed.

For the hydrogenolysis of cellulose into polyols (EG, PG), it is expected that W and Ni species contribute respectively to the retro-aldol cleavage and hydrogenation of unsaturated intermediates.[15] The crystalline phases formed during synthesis as well as their sizes are thus particularly important. Moreover, the formation of NiW alloys may present a positive effect over the catalyst efficiency.[3]

Cellulose hydrogenolysis and cyclability

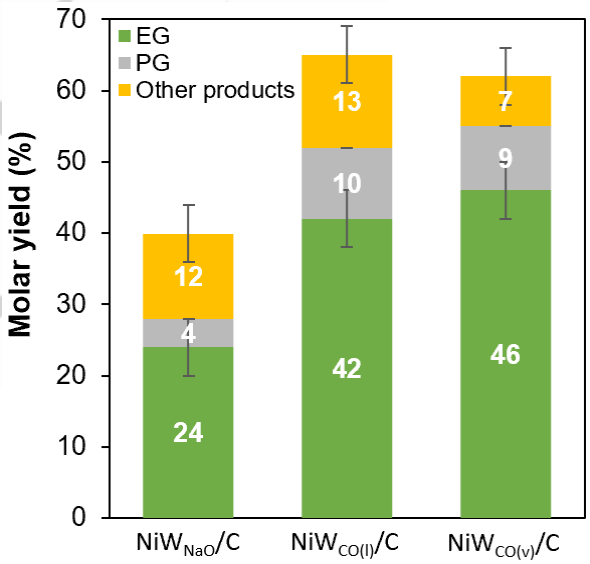

Figure 5. Products molar yields over Ni-W_xC/C catalysts derived from different synthesis pathways. Reaction conditions: 0.50 g cellulose, 0.15 g catalyst, 50 mL water, 60 bar H_2, 1000 rpm, 245 °C, and 1 hour.

Figure 5 and Table S6 display the catalytic results of cellulose hydrogenolysis over the series of Ni-W_xC/C materials. The two catalysts prepared using $W(CO)_6$ as the precursor gave relatively comparable EG and PG yields of 42-46 % and 9-10 %, respectively. The presence of large W_xC particles as seen by SEM does not seem to promote neither the formation of EG nor PG: rather, more sorbitol is obtained. Thus, finely dispersed W-containing particles (NiW alloyed and/or W_xC NPs) are critical to obtain a good catalytic activity. Of note, the carbon balance remains below 70 % with all catalysts, which is due to the formation of oligomeric products arising either from partial

cellulose depolymerization, or formed through recondensation reactions between highly reactive intermediates. These products are most often ill-characterized and therefore not identified enough to be included in the carbon balance.

The catalytic efficiency of all this series falls short of the benchmark catalyst (WC_x/MC), for which cumulated (EG + PG) yields above 70 % are reported.[3-4] On the other hand, the W/Ni weight ratio is far from optimal (0.9 instead of 6) due to the limitations induced by the MOF framework containing a high loading of Ni, and the two NiWCO/C catalysts are performing better than the previous study starting from a MOF.[7] Moreover, to target real-life applications, not only should the catalyst be highly active, but it should also be stable over cycling. Thus, we assessed the stability of the most selective catalyst, $NiW_{CO(v)}$/C, under recycling experiments (Figure 6). The same reaction conditions were applied during each run, without any reactivation treatment in-between. Interestingly, the cumulated yield of glycols remains relatively stable for 2 runs (52-53 %), before a slight loss measured at the third run (45 %) even if the yields remain in the error margin. Hence, at the third run, the catalyst becomes comparable in activity to the benchmark catalysts. To better understand this observation, the reaction solutions were recovered after each run and dissolved metal species were quantified by ICP-OES (Table S7). After the first run, a leaching of 7.4 % of total W and 1.3 % of total Ni was measured. Ni leaching remains stable over the recycling experiments at ± 1 % per run, while W leaching significantly decreases over the three cycles to become close to ± 1 %. This means that after removal of the soluble fraction of W species, the residual W is relatively stable upon leaching. Considering that the change in efficiency is relatively modest between the first and second cycles, it could be assumed that the 7.4 % of dissolved W species are not significantly contributing to the catalysis.

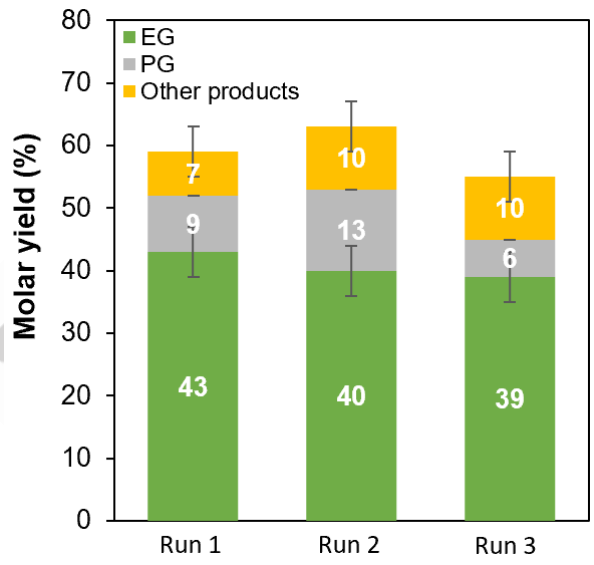

Figure 6. Recycling experiments on the conversion of cellulose into polyols over $NiW_{CO(v)}$/C. Reaction conditions: 0.50 g cellulose, 0.15 g catalyst, 50 mL water, 60 bar H_2, 1000 rpm, 245 °C, and 1 hour.

$NiW_{CO(v)}$/C was also characterized after the three runs. Its XRD pattern is comparable (Figure S17), with the presence of $W_{0.04}Ni_{0.96}$ alloy after reaction along with a small fraction of a crystalline impurity. In addition, applying the Scherrer equation on the diffractogram reflection leads to comparable NiW crystal size (13 nm after reaction, *vs*. 12 nm before reaction). Moreover, the TEM images presented in Figure S18 reveal the presence of two populations of particles, as in the case of the as-pyrolyzed material. However, few larger Ni-rich particles with sizes in the 10-40 nm region are also observed. In all cases, these particles are composed of Ni and W. Thus, only limited sintering of the particles is observed after test (Figure S18c). The textural properties, after reaction, remained close to the values measured on $NiW_{CO(v)}$/C (see Table S8: S_{BET}: 107 $m^2.g^{-1}$ after reaction, vs. 104 $m^2.g^{-1}$ as-pyrolyzed) and the isotherm type remains unchanged (Figure S19). The non-variation of its physico-chemical properties stand behind the resilience of $NiW_{CO(v)}$/C over various catalytic runs.

Conclusion

In summary, we have prepared a series of supported Ni-W_xC on carbon catalysts starting from a nickel-based MOF. The chemical vapor deposition route gave better results in terms of NP size and dispersion, and it also led to the highest polyols yield (55 %) out of the series of catalysts. While it remains slightly below the benchmark catalysts from the literature, its good stability over three consecutive runs with no reactivation procedure rises interest. Our next objective is to decrease the weight percentage of nickel in the starting MOF structure, either by following a metal defects strategy or by increasing the molecular weight of linker molecules.

Experimental section

Synthesis of DUT-8(Ni) and W/DUT-8(Ni)

The synthesis of pure DUT-8(Ni) was derived from published protocols.[16] Two tungsten deposition routes were investigated. In the liquid-mediated incorporation route, the corresponding amount of W precursor ($W(CO)_6$ or $Na_2WO_4.H_2O$) was added to the ligand solution before mixing with the nickel solution for one hour. The mixture was transferred into a PTFE-lined autoclave and heated at 140 °C for 24 h. The recovered powder was washed three times with DMF, and dried overnight at 80 °C.

In the chemical vapor deposition route, the pure DUT-8(Ni) was placed in a glass vial further introduced in a glass bottle containing the corresponding amount of $W(CO)_6$. The bottle was sealed and heated at 85 °C for 24 h then recovered as such.

More details are given in Supporting Information.

Pyrolysis of W/DUT-8(Ni)

The W-loaded materials were pyrolyzed under a flow of N_2 of 100 $mL.min^{-1}$ applying a temperature increase rate of 10 $°C.min^{-1}$

(from RT to 450 °C), then 1 °C.min^{-1} (from 450 °C to 700 °C) with a final dwelling time of 1 h at 700 °C. The samples were finally passivated under a flow of 1 % O_2 in N_2 of 60 mL.min^{-1} at ambient temperature for 6 h. The following nomenclature was adopted hereafter:

- For the liquid-meditated route materials: NiW_{NaO}/C and $NiW_{CO(l)}$/C, depending on the W precursor used.

- For the chemical vapor deposition route material: $NiW_{CO(v)}$/C.

Hydrogenolysis tests

Prior to reaction, the cellulose was dried in an oven under a nitrogen flow at 80 °C for 4 h. The hydrogenolysis reaction was performed in a 100 mL PARR Hastelloy autoclave reactor equipped with a temperature regulation and a mechanical agitation. Typically, a suspension of 0.5 g of cellulose and 0.15 g of catalyst in 50 mL of deionized water was prepared in the autoclave. Afterwards, the autoclave was purged 3 times with 30 bar of Ar then 1 time with 60 bar of H_2. Subsequently, 60 bar of H_2 were introduced, the autoclave was heated to 245 °C and stirred at 1000 rpm, and the reaction lasted for 1 h. The liquid phase after reaction was filtrated over Teflon (0.45 μm) and analyzed with a Shimadzu series 20 HPLC machine (RID, 0.5 mL.min^{-1} of deionized water, CTO-10AS VP, 40 °C). The carbon content in the aqueous phase (TOC) was analyzed with a Shimadzu TOC-VCSH total organic carbon apparatus to estimate the cellulose liquefaction level.

Supporting Information

The authors have cited additional references within the Supporting Information.[16-19]

Acknowledgements

We thank the Agence Nationale de la Recherche for funding (CatReMo ANR-19-CE43-0005). The Chevreul Institute is thanked for its help in the development of this work through the ARCHI-CM project supported by the “Ministère de l’Enseignement Supérieur de la Recherche et de l’Innovation”, the region “Hauts-de-France”, the ERDF program of the European Union and the “Métropole Européenne de Lille. The authors are also grateful for the technical support from Lille University and Ircatech platform of Ircelyon: Olivier Gardoll (thermal and textural analyses) and Laurence Burylo (XRD) from UCCS; Pascal Bargiela (XPS), Pascale Mascunan and Nicolas Bonnet (ICP analysis) from Ircatech.

Keywords: Metal-organic framework • Hierarchical porosity • Cellulose • Hydrogenolysis • Bimetallic nanoparticles

[1] M. Zheng, J. Pang, R. Sun, A. Wang, T. Zhang, *ACS Catal.* **2017**, 7, 1939.
[2] N. Ji, T. Zhang, M. Zheng, A. Wang, H. Wang, X. Wang, J.G. Chen, *Angew. Chem. Int. Ed.* **2008**, 120, 8638.
[3] F. Goc, T. Epicier, N. Perret, F. Rataboul, *ChemCatChem* **2023**, 15, e202201496.
[4] Y. Zhang, A. Wang, T. Zhang, *Chem Commun.* **2010**, 46, 862.
[5] Y.-T. Xu, X. Xiao, Z.-M. Ye, S. Zhao, R. Shen, C.-T. He, J.-P. Zhang, Y. Li, X.-M. Chen, *J. Am. Chem. Soc.* **2017**, 139, 5285.
[6] a) B. Jiang, H. Sun, T. Yuan, W. He, C. Zheng, H.-J. Zhang, J. Yang, S. Zheng, *Energy Fuels* **2021**, 35, 8173; b) W. Chen, J. Pei, C.-T. He, J. Wan, H. Ren, Y. Wang, J. Dong, K. Wu, W.-C. Cheong, J. Mao, X. Zheng, W. Yan, Z. Zhuang, C. Chen, Q. Peng, D. Wang, Y. Li, *Adv. Mater.* **2018**, 30, 1800396; c) J. Kim, G. T. Neumann, N. D. McNamara, J. C. Hicks, *J. Mater. Chem. A* **2014**, 2, 14014.
[7] Y. Yang, W. Zhang, F. Yang, D. E. Brown, Y. Ren, S. Lee, D. Zeng, Q. Gao, X. Zhang, *Green Chem.* **2016**, 18, 3949.
[8] D. Liu, W. Gu, L. Zhou, L. Wang, J. Zhang, Y. Liu, J. Lei, *Chem. Eng. J.* **2022**, 427, 131503.
[9] N. Klein, C. Herzog, M. Sabo, I. Senkovska, J. Getzschmann, S. Paasch, M.R. Lohe, E. Brunner, S. Kaskel, *Phys. Chem. Chem. Phys.* **2010**, 12, 11778.
[10] C. Di Valentin, G. Pacchioni, *Acc. Chem. Res.* **2014**, 47, 3233.
[11] a) M. C. Biesinger, B. P. Payne, L. W. M. Lau, A. Gerson, R. St. C. Smart, *Surf. Interface Anal.* **2009**, 41, 324; b) A.P. Grosvenor, M.C. Biesinger, R. St.C. Smart, N.S. McIntyre, *Surf. Sci.* **2006**, 600, 1771.
[12] M. Besson, P. Gallezot, C. Pinel, *Chem. Rev.* **2014**, 114, 1827.
[13] P. V. Krasovskii, O. S. Malinovskaya, A. V. Samokhin, Y. V. Blagoveshchenskiy, V. A. Kazakov, A. A. Ashmarin, *Appl. Surf. Sci.* **2015**, 339, 46.
[14] S. Zhang, H. Zhang, W. Zhang, X. Yuan, S. Chen, Z.-F. Ma, Chin. *J. Catal.* **2018**, 39, 1427.
[15] K. Fabičovicová, O. Malter, M. Lucas, P. Claus, *Green Chem.* **2014**, 16, 3580.
[16] N. Kavoosi, V. Bon, I. Senkovska, S. Krause, C. Atzori, F. Bonino, J. Pallmann, S. Paasch, E. Brunner, S. Kaskel, *Dalton Trans.* **2017**, 46, 4685.
[17] Y.-T. Xu, X. Xiao, Z.-M. Ye, S. Zhao, R. Shen, C.-T. He, J.-P. Zhang, Y. Li and X.-M. Chen, *J. Am. Chem. Soc.* **2017**, 139, 5285–5288.
[18] a) P. Melix, F. Paesani, T. Heine, *Adv. Theory Simul.* **2019**, 2, 1900098; b) A. Krylov, A. Vtyurin, P. Petkov, I. Senkovska, M. Maliuta, V. Bon, T. Heine, S. Kaskel, E. Slyusareva, *Phys. Chem. Chem. Phys.* **2017**, 19, 32099.
[19] Z. Xing, Z. Ju, Y. Zhao, J. Wan, Y. Zhu, Y. Qiang, Y. Qian, *Sci. Rep.* **2016**, 6, 26146.

Entry for the Table of Contents

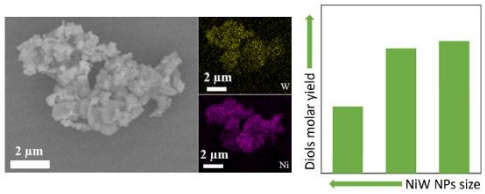

Supported Ni-WxC nanoparticles on carbon were prepared from the pyrolysis of DUT-8(Ni) MOF impregnated with tungsten precursor. The resulting catalysts present a stable activity over several cycles of cellulose hydrogenolysis into diols.

Institute and/or researcher Twitter usernames: @dhainaut_j @UCCS_8181